Inorganic Chemistry
Cite This: Inorg. Chem. 2019, 58, 16629−16641
Article
pubs.acs.org/IC

Structural, Electrochemical, and Magnetic Studies of Bulky Uranium(III) and Uranium(IV) Metallocenes

Michael A. Boreen,[§,†] Daniel J. Lussier,[§,†] Brighton A. Skeel,[§] Trevor D. Lohrey,[§,†] Fabian A. Watt,[#] David K. Shuh,[†] Jeffrey R. Long,[*,§,†,‡,⊥] Stephan Hohloch,[*,#] and John Arnold[*,§,†]

[§]Department of Chemistry, University of California, Berkeley, California 94720, United States
[†]Chemical Sciences Division, Lawrence Berkeley National Laboratory, Berkeley, California 94720, United States
[#]University of Paderborn, Warburger Straße 100, 33098 Paderborn, Germany
[‡]Department of Chemical and Biomolecular Engineering, University of California, Berkeley, California 94720, United States
[⊥]Materials Sciences Division, Lawrence Berkeley National Laboratory, Berkeley, California 94720, United States

Supporting Information

ABSTRACT: Addition of the potassium salt of the bulky tetra(isopropyl)cyclopentadienyl (Cp^{iPr4}) ligand to $UI_3(1,4\text{-dioxane})_{1.5}$ results in the formation of the bent metallocene uranium(III) complex $(Cp^{iPr4})_2UI$ (**1**), which is then used to obtain the uranium(IV) and uranium(III) dihalides $(Cp^{iPr4})_2U^{IV}X_2$ (**2-X**) and [cation]-$[(Cp^{iPr4})_2U^{III}X_2]$ (**3-X**, [cation]$^+$ = $[Cp^*_2Co]^+$, $[Et_4N]^+$, or $[Me_4N]^+$) as mononuclear, donor-free complexes, for X^- = F^-, Cl^-, Br^-, and I^-. Interestingly, reaction of **1** with chloride and cyanide salts of alkali metal ions leads to isolation of the chloride- and cyanide-bridged coordination solids $[(Cp^{iPr4})_2U(\mu\text{-Cl})_2Cs]_n$ (**4-Cl**) and $[(Cp^{iPr4})_2U(\mu\text{-CN})_2Na(OEt_2)_2]_n$ (**4-CN**). Abstraction of the iodide ligand from **1** further enables isolation of the "base-free" metallocenium cation salt $[(Cp^{iPr4})_2U][B(C_6F_5)_4]$ (**5**) and its DME adduct $[(Cp^{iPr4})_2U(DME)][B(C_6F_5)_4]$ (**5-DME**). Solid-state structures of all of the compounds, determined by X-ray crystallography, facilitate a detailed analysis of the effect of changing oxidation state or halide ligand on the molecular structure. NMR spectroscopy, X-ray crystallography, cyclic voltammetry, and UV−visible spectroscopy studies of **2-X** and **3-X** further reveal that the difluoride species in both series exhibit properties that differ significantly from trends observed among the other dihalides, such as a substantial negative shift in the potential of the $[(Cp^{iPr4})_2UX_2]$ uranium(III/IV) redox couple. Magnetic characterization of **1** and **5** reveals that both compounds exhibit slow magnetic relaxation of molecular origin under applied magnetic fields; this process is dominated by a Raman relaxation mechanism.

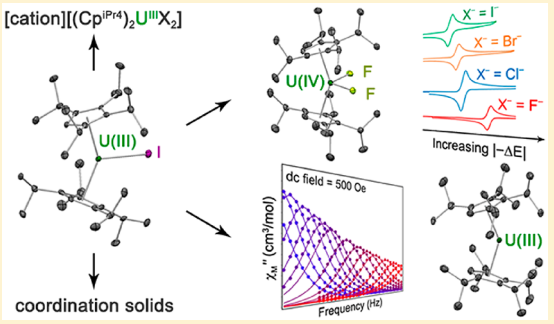

INTRODUCTION

The organometallic chemistry of uranium prominently features complexes containing substituted or unsubstituted cyclopentadienyl ligands, Cp^R.[1−4] In particular, uranium metallocenes featuring the $(Cp^R)_2U$ moiety have supported a large variety of intriguing—and often quite reactive—structural motifs, such as uranium−ligand multiple bonds,[5−11] a uranium−aluminum interaction,[12] uranium(V) complexes,[13−18] cationic uranium(III) species,[19,20] and uranium hydrides.[21−25] In the past few years, bulky $[Cp^R]^-$ ligands have also enabled the synthesis of base-free dysprosium(III) metallocenium cation salts $[(Cp^R)_2Dy][B(C_6F_5)_4]$, which, incredibly, function as single-molecule magnets with magnetic blocking temperatures near and exceeding 77 K, higher than any previously reported systems.[26−29] This synthetic strategy was also very recently extended to the preparation of the uranium(III) metallocenium complex $[(Cp^{iPr5})_2U][B(C_6F_5)_4]$ (Cp^{iPr5} = penta(isopropyl)cyclopentadienyl), which was also found to exhibit slow magnetic relaxation in the presence of an applied magnetic field.[30]

We had simultaneously been interested in studying complexes featuring the $(Cp^{iPr4})_2U$ moiety (Cp^{iPr4} = tetra(isopropyl)cyclopentadienyl), as the Cp^{iPr4} ligand is quite sterically encumbering but less bulky than Cp^{iPr5}, which should enable access to a wide variety of mononuclear complexes without the need for additional donor ligands, while also promoting more facile substitution of equatorial ligands. While metallocene complexes featuring Cp^{iPr4} have been prepared with transition metals,[31−37] s- and p-block metals,[38−40] and the lanthanides,[41−45] the only reported example with uranium is $(Cp^{iPr4})U(BH_4)_3$, which has not been structurally characterized.[46] As an initial demonstration of the utility of the Cp^{iPr4} ligand in uranium chemistry, we were interested in targeting dihalide series for both uranium(III) and uranium(IV).

Received: September 10, 2019
Published: November 26, 2019

Downloaded via UNIV OF CALIFORNIA BERKELEY on January 11, 2020 at 17:29:37 (UTC).
See https://pubs.acs.org/sharingguidelines for options on how to legitimately share published articles.

© 2019 American Chemical Society

DOI: 10.1021/acs.inorgchem.9b02719
Inorg. Chem. 2019, 58, 16629−16641

Scheme 1. Synthesis of the Uranium(III) Monoiodide $(Cp^{iPr4})_2UI$ (1), Uranium(IV) Dihalides $(Cp^{iPr4})_2UX_2$ (2-X), and Uranium(III) Dihalides [cation][$(Cp^{iPr4})_2UX_2$] (3-X) ([cation]$^+$ = $[Cp^*_2Co]^+$, $[Et_4N]^+$, or $[Me_4N]^+$) for X^- = I^-, Br^-, Cl^-, and F^-

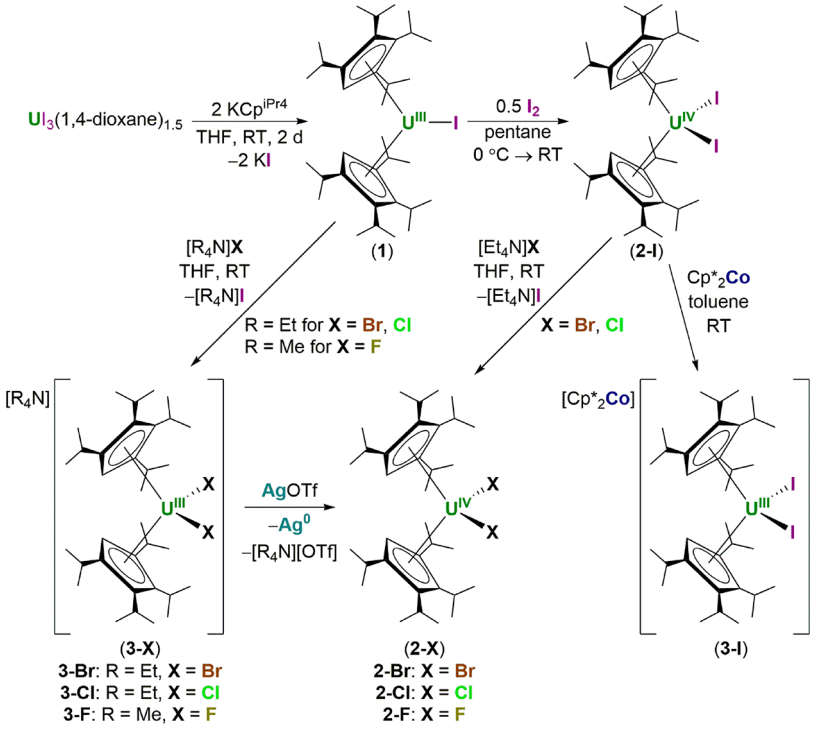

Despite the importance of metallocene dihalide species as starting materials[47] and the usefulness of halides series for analyzing trends in structure and bonding,[16,48,49] no mononuclear, donor-free dihalide series of the form $[(Cp^R)_2UX_2]^-$ or $[(Cp^R)_2UX_2]$ (X^- = F^-, Cl^-, Br^-, I^-) has been structurally characterized.[50] Furthermore, using any kind of ligand, there is only one report of a uranium(III) terminal fluoride complex, Tp^*_2UF (Tp^* = hydrotris(3,5-dimethylpyrazolyl)borate).[51]

Here, we report the uranium(III) complex $(Cp^{iPr4})_2UI$ (**1**) as a versatile synthon for the straightforward synthesis of the uranium(IV) and uranium(III) metallocene dihalide series $[(Cp^{iPr4})_2UX_2]$ (**2-X**) and $[(Cp^{iPr4})_2UX_2]^-$ (**3-X**) (X^- = F^-, Cl^-, Br^-, I^-), as well as the coordination solids $[(Cp^{iPr4})_2U(\mu\text{-}Cl)_2Cs]_n$ (**4-Cl**) and $[(Cp^{iPr4})_2U(\mu\text{-}CN)_2Na(OEt_2)_2]_n$ (**4-CN**). Detailed solution- and solid-state structural analysis of **2-X** and **3-X** using NMR spectroscopy and X-ray crystallography, together with cyclic voltammetry and UV−visible absorption data, indicate that the fluoride analogues exhibit unique properties relative to their respective dihalide congeners. We also isolate and structurally characterize the uranium(III) metallocenium complex $[(Cp^{iPr4})_2U][B(C_6F_5)_4]$ as both a base-free species (**5**) and a Lewis-base adduct with dimethoxyethane (DME) (**5-DME**). Comprehensive magnetic characterization of **1** and **5** reveals fast zero-field magnetic relaxation for both complexes, but unusually slow relaxation, for actinides, under applied fields.

RESULTS AND DISCUSSION

Synthesis of Bis-Cp^{iPr4} Uranium(III) and Uranium(IV) Complexes. The reaction of $UI_3(1,4\text{-dioxane})_{1.5}$ with two equivalents of KCp^{iPr4} at room temperature in THF led, upon workup, to isolation of $(Cp^{iPr4})_2UI$ (**1**) as dark blue crystals in 76% yield (Scheme 1). Notably, related metalation reactions of tetra- and pentaisopropyl Cp ligands with f-block elements have typically involved elevated temperatures.[28,30] While solutions of **1** in THF are green, solutions of **1** in hexamethyldisiloxane (HMDSO), hexane, benzene, toluene, fluorobenzene, ether, and DME are blue. UV−vis spectroscopy confirmed that **1** binds THF in solution (Figure S1), but this bound THF can be readily removed under reduced pressure at room temperature.

Addition of 0.5 equiv of iodine to a pentane solution of **1** afforded the uranium(IV) diiodide $(Cp^{iPr4})_2UI_2$ (**2-I**), as dark red crystals in 67% yield. Complex **2-I** could also be isolated in 61% yield by addition of I_2 to solutions of **1** generated *in situ* in THF. Intriguingly, **2-I** was also isolated from a reaction between **1** and 1 equiv of Me_3SiN_3 (see Experimental Section)—here, it is possible that **2-I** formed by disproportionation of two $(Cp^{iPr4})_2U(NSiMe_3)(I)$ molecules or by comproportionation of $(Cp^{iPr4})_2U(NSiMe_3)(I)$ and **1**, but no other products were isolated from this reaction mixture.

To form a uranium(III) diodide complex, we treated **2-I** with decamethylcobaltocene (Cp^*_2Co, Cp^* = pentamethylcyclopentadienyl) in toluene. A rapid color change occurred from red to green, followed by the precipitation of green crystals of $[Cp^*_2Co][(Cp^{iPr4})_2UI_2]$ (**3-I**) in 84% yield. We next targeted the remaining uranium(III) dihalide species, $[(Cp^{iPr4})_2UX_2]^-$ (X^- = Br^-, Cl^-, F^-). Reaction of **1** with an excess of the appropriate tetraalkylammonium halide salt in THF furnished the dihalide complexes $[Et_4N][(Cp^{iPr4})_2UBr_2]$ (**3-Br**), $[Et_4N][(Cp^{iPr4})_2UCl_2]$ (**3-Cl**), and $[Me_4N][(Cp^{iPr4})_2UF_2]$ (**3-F**) in 76−86% yields. Notably, use of 1 equiv of $[Et_4N][Cl]$ yielded **3-Cl** as the only isolable product, suggesting that this method may not be feasible for synthesizing neutral uranium(III) monohalide species. While **3-Br** and **3-Cl** are green solids like **3-I**, **3-F** is dark purple.

DOI: 10.1021/acs.inorgchem.9b02719
Inorg. Chem. 2019, 58, 16629−16641

Table 1. Selected Distances (Å) and Angles (deg) for 1, 2-X (X^- = I^-, Br^-, Cl^-, F^-), 2-F·pent, 3-X, 4-Cl·Et_2O, 4-CN, 5, and 5-DME

complex	U−X[a]	X−U−X[a]	U−Cp(cent)	Cp(cent)−U−Cp(cent)
1	3.0596(5)	—	2.480(3), 2.510(2)	142.26(8)
2-I	2.9643(7), 2.9727(7)	89.87(2)	2.485(4), 2.491(4)	140.2(1)
2-Br	2.740(1), 2.748(1)	93.16(3)	2.480(4), 2.488(4)	139.8(2)
2-Cl	2.570(1), 2.577(1)	92.45(4)	2.473(2), 2.479(2)	142.97(7)
2-F[b]	2.074(3), 2.085(2)	99.33(8)	2.470(2), 2.478(2)	146.53(6)
2-F·pent[b]	2.086(2), 2.087(3), 2.089(2), 2.090(2)	96.74(8), 98.07(9)	2.483(1), 2.486(1), 2.486(2), 2.489(2)	141.43(5), 141.82(4)
3-I	3.1219(7), 3.1259(7), 3.1354(8), 3.1395(7)	86.54(2), 90.65(2)	2.556(4), 2.556(5), 2.559(4) 2.565(4)	135.6(1), 136.6(2)
3-Br	2.8508(6), 2.8601(6)	90.26(2)	2.543(2), 2.549(1)	138.80(5)
3-Cl	2.782(2), 2.790(2)	91.84(4)	2.545(3), 2.546(3)	140.28(9)
3-F[c]	2.186(8), 2.194(6), 2.194(6), 2.206(3)	89.1(3), 89.6(2)	2.577(6), 2.578(3), 2.589(3), 2.608(7)	137.8(1), 140.0(3)
4-Cl·Et_2O	2.748(5), 2.751(6)	86.8(2)	2.54(1), 2.548(9)	137.2(3)
4-CN	2.537(9), 2.545(9), 2.566(9), 2.570(9)	100.8(3), 102.7(3)	2.525(4), 2.529(4), 2.536(3), 2.542(4)	143.1(1), 144.2(1)
5[c]	–	–	2.410(4), 2.43(1)	142.5(2)
5-DME	2.596(3), 2.550(2)	64.60(8)	2.518(1), 2.558(2)	138.33(6)

[a]X denotes the bound halide ligand, except in **4-CN** and **5-DME**, in which it denotes the cyanide carbons and DME oxygens, respectively. [b]**2-F** was crystallized from HMDSO at −40 °C; **2-F·pent** was crystallized from pentane at −78 °C. [c]Metrics from the minor disordered component are not given.

To prepare the remaining uranium(IV) dihalide compounds, we hypothesized that oxidation of **3-X** and halide exchange from **2-I** would both be viable synthetic routes. Clean oxidation of **3-X** to **2-X** with AgOTf was observed in diethyl ether, and **2-X** (X^- = Br^-, Cl^-, F^-) could be isolated in 64−67% yields even using crude **3-X** generated from halide exchange starting with **1**. The reaction of **2-I** with $[Et_4N][X]$ (X^- = Br^-, Cl^-) also proceeded cleanly with isolated yields of 87% (**2-Br**) and 81% (**2-Cl**). Curiously, however, very little conversion was observed when **2-I** and $[Me_4N][F]$ were allowed to react under similar conditions, and it was only possible to isolate **2-F** via oxidation of **3-F**. Attempts to prepare **2-I** or **2-Cl** from the reaction of KCp^{iPr4} with $UI_4(OEt_2)_2$ or UCl_4, respectively, led to intractable mixtures. In the former case, significant quantities of **1** were observed to form by ^{1}H NMR spectroscopy, indicating that reduction to uranium(III) occurs faster than ligand substitution. Complexes **2-Br** and **2-Cl** have a red-brown color, while **2-F** has a red-orange color.

Interestingly, we also found that reaction of **1** with alkali metal halides or pseudohalides leads to the formation of crystals containing extended structures, as the alkali metal cations are significantly more coordinating than the tetraalkylammonium ions (Scheme S1). Specifically, reaction of **1** with CsCl or NaCN yielded $[(Cp^{iPr4})_2U(\mu\text{-}Cl)_2Cs]_n$ (**4-Cl**) or $[(Cp^{iPr4})_2U(\mu\text{-}CN)_2Na(OEt_2)_2]_n$ (**4-CN**), respectively. The cyanide ligands in **4-CN** were all assigned as C-bound to uranium, based on the X-ray crystallographic data (see below), given that more reasonable thermal parameters and lower *R* values were found following refinement in this orientation versus N-bound coordination. Furthermore, while actinide complexes have been isolated featuring N-bound isocyanide (NC^-) ligands,[52−54] the C-bound orientation has exclusively been observed for uranium(III) species. The C−N stretch of **4-CN** was observed at 2102 cm^{-1}, similar to cyanide C−N stretches at 2088 and 2082 cm^{-1} for the bridging uranium(III) cyanide complexes $[Cp^*_2U(CN^tBu)(\mu\text{-}CN)]_3$ and $[Cp^*_2U(\mu\text{-}CN)]_n$, respectively.[55−57] Both **4-Cl** and **4-CN** are green solids that dissolve in diethyl ether to form green solutions. While **4-CN** reacts rapidly with oxidants such as AgOTf to form dark red solutions, we were unable to isolate a neutral uranium(IV) dicyanide complex.

The strongly electrophilic silylium compound $[(Et_3Si)_2(\mu\text{-}H)][B(C_6F_5)_4]$[58] was recently used to abstract the iodide ion from $(Cp^{iPr5})_2UI$ to form the base-free uranium(III) metallocenium salt, $[(Cp^{iPr5})_2U][B(C_6F_5)_4]$,[30] and related base-free dysprosium(III) metallocenium salts have been prepared in a similar fashion.[26,28] Addition of $[(Et_3Si)_2(\mu\text{-}H)][B(C_6F_5)_4]$ to a hexane solution of **1** led to precipitation of a dark blue oily product, which could be crystallized from diethyl ether in 61% yield. Elemental analysis of the product was consistent with the formulation of the dark blue crystals as the base-free uranium(III) metallocenium complex $[(Cp^{iPr4})_2U][B(C_6F_5)_4]$ (**5**, Scheme 2). Complex **5** reacts rapidly with coordinating solvents such as THF, and we therefore reasoned that adding a chelating base would lead to a more stable species that would be easier to handle. Addition of excess DME to a crude suspension of **5** in hexane caused a rapid change in color of the solid material from dark blue to green. Green crystals of $[(Cp^{iPr4})_2U(DME)][B(C_6F_5)_4]$ (**5-DME**) were obtained in 79% yield by cooling a layered mixture of hexane and DME to −40 °C.

X-ray Crystallographic Studies. The solid-state structures of all compounds were determined by X-ray crystallography (Figures 1, 2, and S2−S7) and selected bonding metrics are listed in Table 1. In general, the $(Cp^{iPr4})_2U$ fragment maintains the expected bent geometry (Cp(cent)−U−Cp(cent) angles ranging from 135.6(1) to 146.53(6)°), in which the unsubstituted C−H bonds on the Cp^{iPr4} rings are orientated away from the other ligands to minimize steric clashing, as has been observed in similar lanthanide bis-Cp^{iPr4} complexes.[43−46]

While the complex ions of **2-X**, **3-X**, and **5** do not exhibit any crystallographic symmetry, they are all roughly C_2 symmetric with the exception of **3-F**, which has two $[(Cp^{iPr4})_2UF_2]^-$ anions in the asymmetric unit, one with approximate C_2 symmetry and the other with no approximate symmetry. Complex **1** is somewhat more distorted from exact C_2 symmetry, while the two Cp^{iPr4} ligands of **5-DME** are in different conformations, precluding assignment of any approximate symmetry.[59]

DOI: 10.1021/acs.inorgchem.9b02719
Inorg. Chem. 2019, 58, 16629−16641

Scheme 2. Synthesis of the Base-Free Uranium(III) Metallocenium complex $[(Cp^{iPr4})_2U][B(C_6F_5)_4]$ (5) and the DME Adduct $[(Cp^{iPr4})_2U(DME)][B(C_6F_5)_4]$ (5-DME)

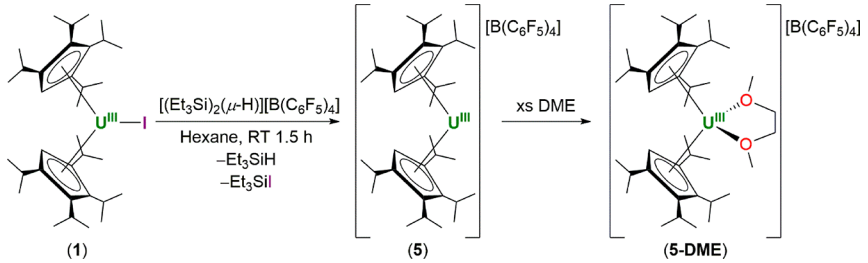

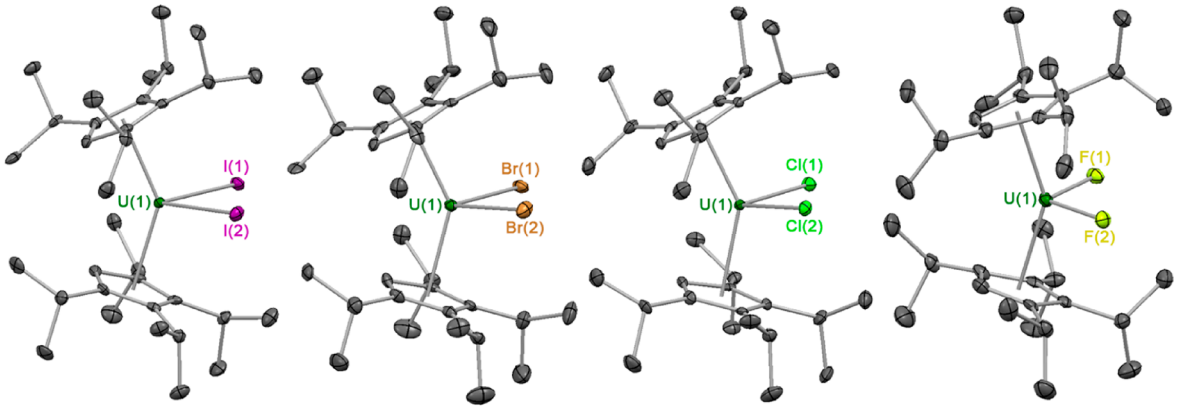

Figure 1. X-ray crystal structures of $(Cp^{iPr4})_2UX_2$ (**2-X**) with 50% probability ellipsoids. From left to right, **2-I**, **2-Br**, **2-Cl**, and **2-F** are shown. Hydrogen atoms are omitted for clarity. Selected structural metrics are listed in Table 1.

Complexes **4-Cl** and **4-CN** crystallize as coordination solids, containing extended one-dimensional chains. Only a small number of metallocene uranium 1D- and 2D-coordination solids have been reported, and these species all feature bridging cyanide or bromide ligands.[56,60,61] In **4-Cl**, there is a single $[(Cp^{iPr4})_2UCl_2]^-$ fragment with approximate C_2 symmetry (Figures S4 and S5), while in the asymmetric unit of **4-CN**, there are two $[(Cp^{iPr4})_2U(CN)_2]^-$ fragments that contain different ligand conformations and thus do not approach any symmetry (Figures S6 and S7).

On the basis of the metrics in Table 1, it is difficult to identify definitive structural trends within the **2-X** and **3-X** series. This problem is highlighted in two different structures determined for **2-F**, one using crystals grown from HMDSO at −40 °C with no solvent in the crystal lattice (**2-F**, Figure 1) and the other using crystals grown from pentane at −78 °C with an equivalent of pentane incorporated in the lattice (**2-F·pent**, Figure S2). Of note is the nearly 5° difference in average Cp(cent)−U−Cp(cent) angles between these two structures, which appears attributable only to differences in crystal packing effects; we note that London dispersion forces in particular may affect the solid-state geometries with such bulky ligands.[62] This difference between the **2-F** structures suggests that the potential well for the Cp(cent)−U−Cp(cent) angle is likely quite shallow and that minor, unpredictable energetic differences can lead to large changes in geometry. Indeed, crystal packing has been noted to have significant effects on this angle in main group and lanthanide metallocene complexes.[63,64]

A comparison of **2-X** with their **3-X** analogs reveals expected bond lengthening upon reduction from uranium(IV) to uranium(III).[65] Additionally, the average X−U−X and Cp(cent)−U−Cp(cent) angles decrease (slightly in most cases) upon going from **2-X** to **3-X** for the same halide ligand, as expected based on the larger size of the uranium(III) ion. Solid-state structures containing isolated anionic uranium(III) fragments of the form $[(Cp^R)_2UX_2]^-$ are quite uncommon,[66−68] but in known complexes, there is little change in the X−U−X angle relative to that in analogous uranium(IV) $(Cp^R)_2UX_2$ species.[69−71] Additionally, the Cp(cent)−U−Cp(cent) angle in these compounds has been found to be larger in the uranium(III) anionic fragment for $[Cp^{‡}_2UCl_2]^-$ ($Cp^{‡}$ = 1,3-$(SiMe_3)_2C_5H_3$)[66] but smaller in $[Cp^*_2UI_2]^-$[67] and $[(Cp^{tet})_2UCl_2]^-$ (Cp^{tet} = C_5Me_4H)[68] relative to the corresponding neutral uranium(IV) species.

In a series of cycloheptatrienyl zirconium complexes featuring substituted Cp ligands, Walter and co-workers previously found increasing steric demand in the order Cp″ (1,3-$(^tBu)_2C_5H_3$) < Cp* < Cp^{ttt} (1,2,4-$(^tBu)_3C_5H_2$) < Cp^{iPr4} < Cp^{iPr5}.[72] With the first reported structures containing the $(Cp^{iPr4})_2U$ moiety in hand, we were interested in whether these steric differences among Cp ligands might also manifest in similar trends in the corresponding Cp(cent)−U−Cp(cent) angles. We found that similar Cp(cent)−U−Cp(cent) angles occur between **2-Cl** (142.97(7)°) and **2-F** (146.53(6) in **2-F** and 141.63(5)° (avg.) in **2-F·pent**) and their analogs $Cp^{ttt}_2UCl_2$ (145°) and $Cp^{ttt}_2UF_2$ (144°).[8,73] The Cp(cent)−U−Cp(cent) angles in $Cp^*_2UX_2$ (136.4(2)°, 137.6(2)°, and 138° for X^- = I^-,[70] Br^-,[60] and Cl^-,[74] respectively) are only slightly smaller than in their Cp^{iPr4} analogs (140.2(1)°, 139.8(2)°, and 142.97(7)° for **2-I**, **2-Br**, and **2-Cl**, respectively), while significantly smaller angles occur in Cp''_2UF_2 (128.1°) and Cp''_2UCl_2 (125.3°).[69] For all of these compounds, only minor differences are observed in the U−X bond distances for a given halide, despite large changes in the Cp steric profile.

DOI: 10.1021/acs.inorgchem.9b02719
Inorg. Chem. 2019, 58, 16629−16641

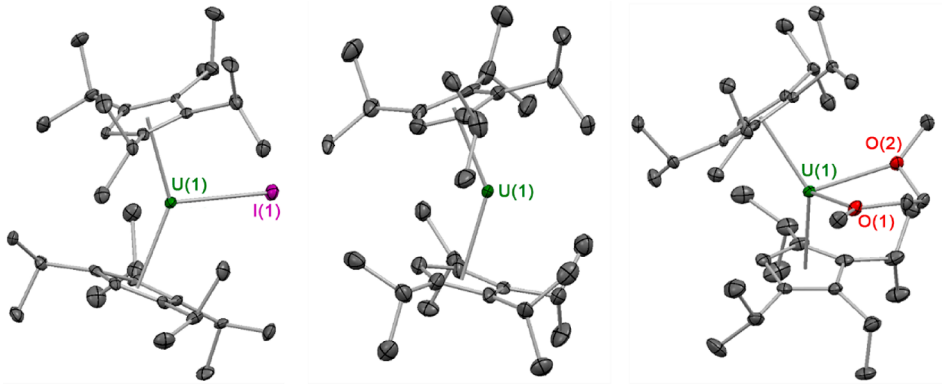

Figure 2. X-ray crystal structures of $(Cp^{iPr4})_2UI$ (**1**) (left) and the metallocenium cations in $[(Cp^{iPr4})_2U][B(C_6F_5)_4]$ (**5**) (middle) and $[(Cp^{iPr4})_2U(DME)][B(C_6F_5)_4]$ (**5-DME**) (right) with 50% probability ellipsoids. Hydrogen atoms, solvent molecules, and the minor disordered component of **5** are omitted for clarity. Selected structural metrics are shown in Table 1.

The Cp(cent)−U−Cp(cent) angles in **1** (142.26(8)°) and **5** (142.5(2)°) are both considerably smaller than those of $(Cp^{iPr5})_2UI$ and $[(Cp^{iPr5})_2U][B(C_6F_5)_4]$ (152.63(6)° and 167.82(8)°, respectively).[30] It is striking that for Cp^{iPr5}, an approximately 15° increase in this angle is observed upon abstraction of the iodide ion from $(Cp^{iPr5})_2UI$, while effectively no change is observed in the system with Cp^{iPr4}. Coordination of the bidentate ligand DME to **5** to form **5-DME** further causes this angle to decrease to 138.33(6)°.

Overall, these results highlight the likelihood of observing shallow potential energy wells for Cp(cent)−U−Cp(cent) bond angles in uranium bent metallocenes,[1] as has been established in calculations of main group and lanthanide metallocenes.[63] These bond angles may be especially prone to large variability in cases where nonbulky substituents, or no substituents, are bound to the metallocene fragment.

NMR Studies. Variable-temperature ^{1}H NMR spectra of **2-F** in toluene-d_8 (Figure S17) reveal that the complex exhibits a range of solution-state behaviors, and the data can be used to elucidate the room temperature ^{1}H NMR spectra of other complexes containing the $(Cp^{iPr4})_2U$ fragment. At 60 °C (Figure S18), seven signals (four methyl groups, two methine protons, and one proton on the Cp^{iPr4} ring) were observed for **2-F**, corresponding to effective C_{2v} molecular symmetry in solution. For this symmetry to be observed, the two Cp^{iPr4} ligands must be made equivalent by a C_2 axis, and each Cp^{iPr4} ligand must rotate rapidly about the uranium−centroid axis to afford a plane of symmetry bisecting the ring. We note that while none of the solid-state structures discussed here contain a crystallographically imposed C_2 axis, most are nearly C_2 symmetric (*vide supra*); furthermore, a partial rotation of the Cp^{iPr4} ligand is sufficient to yield an apparent plane of symmetry, as shown in Figure S24.[75]

Upon cooling from 60 °C, the signals for **2-F** broaden considerably until a coalescence temperature between 0 and 10 °C, below which 13 signals (eight methyl groups, four methine protons, and one proton on the Cp^{iPr4} ring) are observed; these resonances sharpen as the temperature is lowered (Figure S19). This change corresponds to a loss of rapid Cp^{iPr4} ring rotation and therefore a change in effective solution symmetry to C_2. At −30 °C, a new broad peak appears at ca. −48 ppm, and this signal sharpens at lower temperatures while many other new peaks gradually grow in and sharpen. At −80 °C (Figure S20), approximately 50 new signals are observed and span a range of chemical shifts similar to the C_2 symmetric **2-F** monomer. We attribute these new peaks to the presence of a dimer with C_1 symmetry, as such a species would be expected to exhibit 52 resonances. For comparison, we note that dimerization of Cp''_2UF_2 and $Cp^{\ddagger}_2UF_2$ has been observed in solution at low temperatures.[69] Furthermore, $Cp^{\ddagger}_2UF_2$ crystallizes as a dimer, while $Cp^{\ddagger}_2UX_2$ (X^- = Cl^-, Br^-, and I^-) are monomeric in the solid-state.[69,76] Presumably, the small size and high charge density of the fluoride ion relative to the other halides facilitates dimerization.[69]

Analysis of the variable-temperature ^{1}H NMR spectra of **2-Cl** in toluene-d_8 (Figure S21) provides additional support for the above analysis of the solution dynamics of **2-F**. At high temperatures, the ^{1}H NMR spectrum of **2-Cl** contains seven signals (Figure S22), while at low temperatures, 13 signals are observed (after accounting for overlapping signals, see Figure S23), and no evidence of dimerization is observed at temperatures down to −80 °C. Similar to **2-F**, complex **2-Cl** undergoes a transition from C_{2v} to C_2 symmetry, but at a higher temperature within the range of ∼40−50 °C; the larger size of chloride relative to fluoride likely hinders ring rotation and therefore increases the barrier associated with this motion.

Plots of chemical shift (δ) versus reciprocal temperature ($1/T$) are linear for the sets of protons in **2-F** and **2-Cl**, indicating that the molecules follow Curie behavior within each temperature region (see Figure S25). However, a significant change in slope is observed near the coalescence temperature for the $C_5(^i\mathrm{Pr})_4H$ proton in **2-F**, consistent with a change in the time-averaged pseudocontact shift experienced by the proton as the molecule undergoes the ring rotation that gives rise to the effective molecular C_{2v} symmetry in solution (Figure S24). See the explanation of Figure S25 in the Supporting Information for further discussion and comparison to **2-Cl**.

Complexes **2-I**, **2-Br**, and **2-Cl** all have qualitatively similar room temperature C_2 symmetric ^{1}H NMR spectra, notably distinct from the C_{2v}-symmetric room temperature spectrum for **2-F**. Interestingly, the line widths increase significantly from **2-I** to **2-Br** to **2-Cl** (Figures S9−S11), suggesting that dynamic behavior (ring rotation) is slowest in **2-I**. However, the line widths of **2-I** are still larger than those typically observed for cyclopentadienyl ligands bound to uranium(IV) at room temperature (see the Experimental Section for line widths for each compound).[69,77] These observations suggest that the barrier to ring rotation in **2-X** consistently increases as the size of the halide increases.[78]

DOI: 10.1021/acs.inorgchem.9b02719
Inorg. Chem. 2019, 58, 16629−16641

The room temperature ^{1}H NMR spectrum of **3-I** in pyridine-d_5 contains 13 Cp^{iPr4} signals, indicating that the $[(Cp^{iPr4})_2UI_2]^-$ ion adopts C_2 symmetry in solution at this temperature (Figure S13). Resonances for Cp ligands bound to uranium(III) are typically broader than those of uranium(IV) analogs,[77] and indeed the line widths of **3-I** are larger than those of **2-I**. Interestingly, the line widths of **3-I** are also larger than commonly observed for uranium(III)−Cp^R species, likely as a result of Cp^{iPr4} ring rotation.[75,77]

As observed in the **2-X** series, the ^{1}H NMR line widths for the **3-X** series increase successively from **3-I** to **3-Br** to **3-Cl** (Figures S13−S15), suggesting faster solution dynamics (and a lower barrier to Cp^{iPr4} ring rotation) as the halide size decreases. Moreover, at room temperature, **3-Cl** appears to be very close to its coalescence temperature, based on a qualitative comparison to the spectra of **2-F** and **2-Cl** near their respective coalescence temperatures. In contrast, at room temperature, **2-Cl** is far enough below its coalescence temperature for its symmetry to be well-defined. This distinction suggests a lower barrier to Cp^{iPr4} ring rotation in **3-Cl** than in **2-Cl**, as would be expected given the larger size of the uranium(III) ion relative to uranium(IV).

Compound **3-F** was observed to react with pyridine, so NMR data for this compound was acquired in C_6D_6, despite its low solubility in this solvent (Figure S16). While use of a different NMR solvent complicates comparisons between **3-F** and the rest of the **3-X** series, the room temperature ^{1}H NMR spectrum of **3-F** contains fewer and sharper resonances, suggesting that the $[(Cp^{iPr4})_2UF_2]^-$ complex ion is C_{2v} symmetric and well above its coalescence temperature. This result is consistent with the proximity of **3-Cl** to its coalescence temperature near room temperature, as coalescence temperature is expected to decrease as the size of the halide decreases, due to more facile ring rotation.

Evidence for ion pairing was also observed by ^{1}H NMR spectroscopy in the **3-X** series. The spectrum of **3-I** in pyridine-d_5 contains a relatively sharp singlet at 0.97 ppm (line width = 12.8 Hz) corresponding to the 30 protons of the $[Cp^*_2Co]^+$ cation; in comparison, $[Cp^*_2Co][PF_6]$ in acetone-d_6 and $[Cp^*_2Co][B(3,5\text{-}(CF_3)_2C_6H_3)_4]$ in THF-d_8 display $[Cp^*_2Co]^+$ signals at 1.78 and 1.75 ppm, respectively, suggesting some degree of shifting due to ion pairing in **3-I** in pyridine solution.[79,80]

The $[Et_4N]^+$ cations in **3-Br** and **3-Cl** exhibit signals with line widths of 20−25 Hz with chemical shifts of 1.00 (methylene) and −0.54 ppm (methyl) for **3-Br** and 1.55 (methylene) and −0.15 ppm (methyl) for **3-Cl** (Figure S14 and S15 insets, respectively). The methylene signal in **3-Cl** is split into a quartet, while the other three above-mentioned resonances appear as slightly broadened singlets. Typical ^{1}H chemical shifts for $[Et_4N][Br]$ and $[Et_4N][Cl]$ in various solvents are 3.2−3.5 and 1.2−1.5 ppm for the methylene and methyl resonances, respectively.[81−83] Therefore, ion pairing leads to greater pseudocontact shifts in the $[Et_4N]^+$ resonances in **3-Br** than in **3-Cl**.[84,85] While the solubility of **3-Cl** in C_6D_6 was too low to see the Cp^{iPr4} signals in the ^{1}H NMR spectrum, the $[Et_4N]^+$ resonances were observed as singlets at −8.64 (methylene) and −7.19 ppm (methyl), consistent with expected stronger ion pairing in the less polar solvent, benzene. The line widths for the $[Et_4N]^+$ resonances in **3-Cl** are effectively unchanged between pyridine-d_5 and C_6D_6. The $[Me_4N]^+$ peak of **3-F** was tentatively assigned to the resonance at 4.74 ppm, based on its smaller line width (66 Hz) relative to the other resonances in the ^{1}H spectrum; for comparison, the ^{1}H signal for $[Me_4N]^+$ in $[Me_4N][^nBu_4B]$ in C_6H_6 was reported at 2.05 ppm.[86]

Only six resonances could be identified in the ^{1}H NMR spectrum of **1** at room temperature (Figure S8), and thus the molecule likely exhibits an effective C_{2v} symmetry in solution at this temperature. The extreme broadness of multiple signals again suggests fast dynamics in solution, which may be facilitated by the open coordination site on the uranium(III) center.

Cyclic Voltammetric Studies of the U(III)/U(IV) Redox Couple in $[(Cp^{iPr4})_2UX_2]^{0/-1}$ (X^- = I^-, Br^-, Cl^-, and F^-). Cyclic voltammograms of **2-X** (X^- = I^-, Br^-, Cl^-, F^-) were recorded in THF using $[^nBu_4N][B(C_6F_5)_4]$ as the supporting electrolyte (see Supporting Information for details). For each compound, the only feature observed in the electrochemical window was the uranium(III/IV) redox couple, which was reversible for all four species (Figure 3). We note that cyclic voltammograms obtained using $[^nBu_4N][PF_6]$ as the electrolyte featured only quasi-reversible or irreversible redox waves, a phenomenon reported previously in the study of actinide electrochemistry when using electrolytes containing PF_6^- or BF_4^- anions.[87]

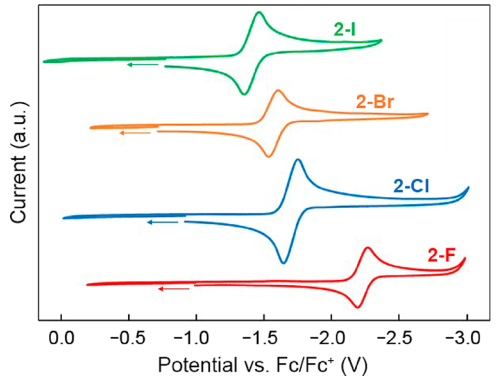

Figure 3. Cyclic voltammograms of **2-X** carried out in THF with 0.2 M $[^nBu_4N][B(C_6F_5)_4]$ electrolyte (scan rate = 100 mV/s). The $E_{1/2}$ values for each uranium(III/IV) redox couple versus the ferrocene/ferrocenium (Fc/Fc^+) redox couple are −1.41, −1.57, −1.70, and −2.23 V for **2-I**, **2-Br**, **2-Cl**, and **2-F**, respectively.

The $E_{1/2}$ values for each uranium(III/IV) redox couple (versus the ferrocene/ferrocenium redox couple) were found to be −1.41, −1.57, −1.70, and −2.23 V for **2-I**, **2-Br**, **2-Cl**, and **2-F**, respectively (Figure 3). Intriguingly, while the values shift by only 130−160 mV from **2-I** to **2-Br** and from **2-Br** to **2-Cl**, the negative shift in $E_{1/2}$ from **2-Cl** to **2-F** is significantly larger (530 mV). Kiplinger and co-workers observed a similar effect on the uranium(III/IV) couple in the series of complexes $Cp^*_2U[N(SiMe_3)_2](X)$ (X^- = Br^-, Cl^-, F^-; 70 versus 310 mV upon switching from bromide to chloride versus chloride to fluoride, respectively).[49] Similar effects upon switching from chloride to fluoride have also been observed for the U(IV/V), U(V/VI), and Ce(III/IV) couples in a variety of complexes, although the effect in **2-X** is particularly pronounced due to the presence of two halides.[14,16,49,88] To rule out coordination of THF as an influence on our electrochemical measurements, ^{1}H NMR spectra of **2-F** in C_6D_6 were recorded before and after adding a drop of THF, and no difference was observed between the spectra (Figure S26). The anomalously large effect of the fluoride ligand on stabilizing the higher oxidation

DOI: 10.1021/acs.inorgchem.9b02719
Inorg. Chem. 2019, 58, 16629−16641

state can be attributed to its ability to engage in both strong covalent and electrostatic interactions with uranium; in particular, fluoride acts as a stronger π-donor than the other halides.[89−91] The overall halide trend we observe is also consistent with hard−soft acid−base theory: the larger, more polarizable halides better stabilize the lower oxidation state.[16]

UV−Visible Absorption Spectra of $(Cp^{iPr4})_2UX_2$ and $[(Cp^{iPr4})_2UX_2]^-$. UV−visible absorption spectra of **2-X** and **3-X** were recorded in THF (Figure 4). Each compound in the **2-X** series displays an intense (ε_{max} = 3420−4320 $M^{-1}\cdot cm^{-1}$) band near or into the UV region (λ_{max} = 333−443 nm). Given the intensities and the shifts to lower energies for heavier halides in **2-X** (Table 2), we assigned these as ligand-to-metal charge transfer (LMCT) bands. The UV−vis spectrum of **2-Cl** is qualitatively similar to that of $Cp^*_2UCl_2$, which displays a band at approximately 26000 cm^{-1} (385 nm) with a maximum intensity slightly greater than 3000 $M^{-1}\cdot cm^{-1}$ in toluene.[87] Notably, no such band was observed for $Cp^*_2U(CH_3)_2$,[87] as the methyl electrons are not energetically accessible for an LMCT process.

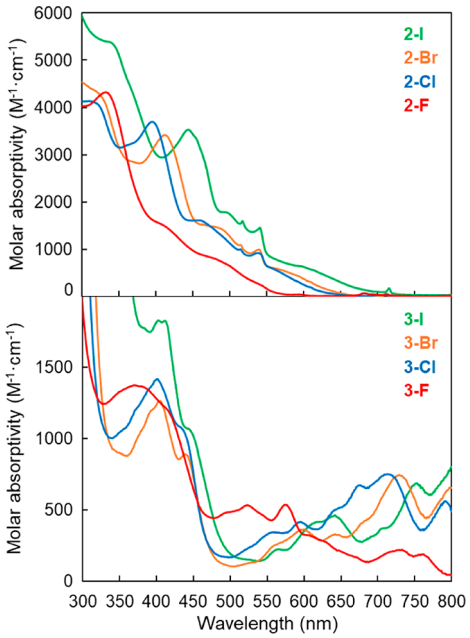

Figure 4. UV−visible spectra of **2-X** (top) and **3-X** (bottom) in THF.

Table 2. Experimental Energies and Intensities of the LMCT Band of 2-X Dissolved in THF

complex	λ_{max} (nm), ν_{max} (cm^{-1})	ε_{max} ($M^{-1}\cdot cm^{-1}$)
2-I	443, 22600	3530
2-Br	412, 24300	3420
2-Cl	394, 25400	3700
2-F	333, 30100	4320

Similar to what was observed above for the change in the uranium(III/IV) redox potential upon going from **2-Cl** to **2-F**, the energy of the LMCT band increases significantly in magnitude upon going from **2-Cl** to **2-F**, relative to the increase from **2-I** to **2-Br** or **2-Br** to **2-Cl**. Such a large difference may explain why uranium(IV) metallocene difluorides have been observed to be different colors than their heavier dihalide analogs.[69]

The visible regions of **3-X** and **1** display a variety of bands generally assigned as 5f−6d transitions, which are typically observed in uranium(III) complexes at wavelengths ranging from ∼500 to 700 nm.[1] A particularly intense absorption for **3-I** occurring at the edge of the visible to within the UV region can be ascribed to the $[Cp^*_2Co]^+$ cation.[92]

Magnetic Studies. The unique coordination environment provided by rigid η^5-cyclopentadienyl ligands has led to remarkable magnetic properties in lanthanide complexes;[26−29,93−95] this can be attributed to the constrained number of metal−ligand vibrational modes that limit the possible pathways for fast, through-barrier magnetic relaxation.[27,29] Through-barrier processes, such as quantum tunneling and Raman relaxation, tend to dominate magnetic relaxation in actinide-based systems,[96−103] although it was recently predicted that the cation $[Cp^{ttt}_2U]^+$ should be capable of relaxing via an Orbach (overbarrier) process.[104] Furthermore, the increased spin−orbit coupling of the 5f orbitals imparts the actinides with greater magnetic anisotropy than the lanthanides, which can, in principle, lead to larger barriers to magnetic relaxation.[96−98,105] However, the Cp^{iPr5} analogue of the uranium metallocenium cation, $[(Cp^{iPr5})_2U][B(C_6F_5)_4]$, and its iodide adduct, $(Cp^{iPr5})_2UI$, were recently shown to exhibit relatively fast, field-induced slow magnetic relaxation via a Raman process.[30] We were therefore interested in a comparison study of the magnetic properties of **1** and **5** in order to shed further light on the magnetization dynamics of the uranium metallocenium cation.

Variable-temperature direct current (dc) magnetic susceptibility measurements were performed on powdered, polycrystalline samples of **1** and **5** (Figures S31 and S32). Under an applied field of 0.1 T, the $\chi_M T$ values of **1** and **5** at 300 K are 1.41 and 1.75 $cm^3\cdot K\cdot mol^{-1}$, respectively, within the range reported for other uranium(III) complexes.[106] The $\chi_M T$ value for **5** is slightly greater than the calculated value of 1.64 $cm^3\cdot K\cdot mol^{-1}$ for a free, noninteracting uranium(III) ion ($5f^3$, $^4I_{9/2}$) as a result of a contribution from temperature independent paramagnetism. This contribution can be suppressed under stronger magnetic fields ($H_{dc} \geq 1$ T), such that, for example, the 300-K $\chi_M T$ value at 5 T is 1.56 $cm^3\cdot K\cdot mol^{-1}$ for **5**. The smaller magnitude of the experimental room temperature $\chi_M T$ value for each complex relative to the calculated free-ion value is typical of actinide complexes and can be ascribed to their large magnetic anisotropies, which cause an unequal thermal population of excited crystal field states.[107]

The relaxation dynamics of polycrystalline **1** and **5** were studied by carrying out alternating current (ac) magnetic susceptibility measurements in the presence of either a 4 or 6 Oe ac field (1−1500 Hz) and zero dc field. Compound **1** exhibited no signal in the out-of-phase susceptibility (χ'') under these conditions (Figure S33), but partial χ'' peaks were observed at high frequency for compound **5** between 1.8 and 3 K (Figures S35 and S36). Although the absence of full χ'' peaks precluded an accurate fit using a generalized Debye model,[108] the relaxation is clearly rapid. We note that there is a slight increase in the magnitude of χ'' with temperature under zero field, behavior that has been characterized previously for other single-molecule magnets.[109,110] Application of a small dc field (*vida infra*) gives rise to full χ'' peaks exhibiting expected behavior (a decrease in the magnitude of χ'' with increasing temperature), and thus, the behavior under zero applied field may arise as a result of intermolecular interactions that serve to partially "freeze" the molecular magnetic moments and are

DOI: 10.1021/acs.inorgchem.9b02719
Inorg. Chem. 2019, 58, 16629−16641

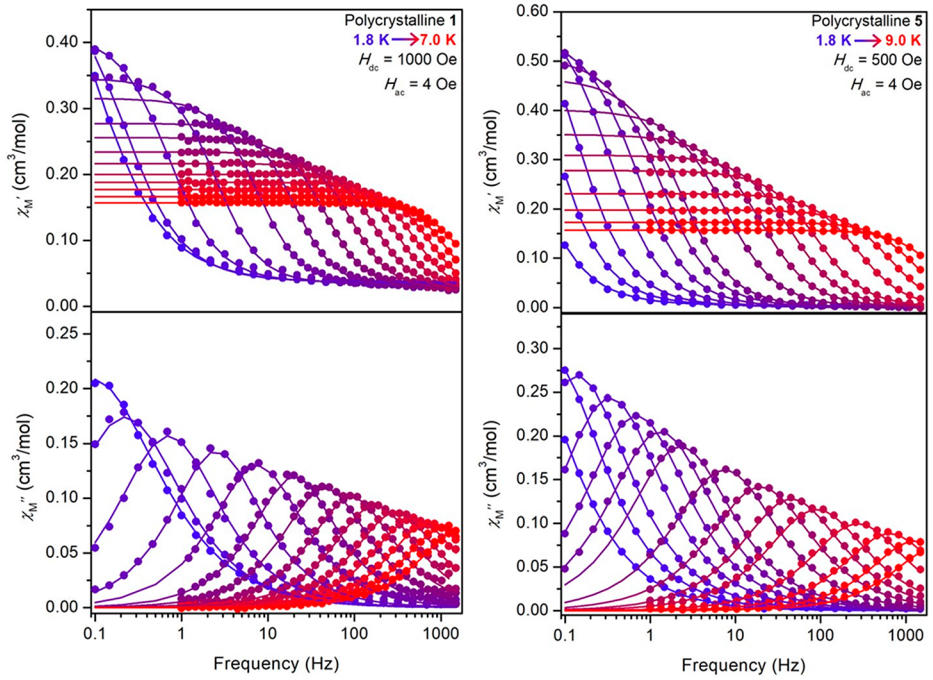

Figure 5. Plots of the in-phase (χ_M') and out-of-phase (χ_M'') molar magnetic susceptibility versus frequency of the oscillating field (4 Oe, 0.1−1500 Hz) for polycrystalline samples of $(Cp^{iPr4})_2UI$ (**1**, left) and $[(Cp^{iPr4})_2U][B(C_6F_5)_4]$ (**5**, right) under static fields of 1000 and 500 Oe, respectively, over the temperature range of 1.8 to 9.0 K. Experimental data points are represented by colored circles, and the points representing fits to a generalized Debye model[108] are connected by solid lines.

disrupted at higher temperatures. The absence of molecular-based slow-magnetic relaxation under zero-field is typical for mononuclear actinide complexes, and arises from efficient quantum tunneling.[30,104,111]

Application of a field suppresses this fast zero field process and results in the emergence of significantly slower, field-activated magnetic relaxation for both **1** and **5** (Figures S33, S34, and S37−S40). Under optimized dc fields of 1000 and 500 Oe for **1** and **5**, respectively, a temperature-dependent χ'' signal was observed for both complexes at temperatures as high as 9.0 K, consistent with molecular magnetic relaxation processes (Figure 5).

The magnetic relaxation times and temperature dependence for the field-activated relaxation processes of **1** and **5** are quite similar to each other (Figure 6), and notably, the relaxation times are significantly longer, by at least an order of magnitude, than those for the other mononuclear actinide-based single-molecule magnets.[30,96,99] Ac measurements (H_{dc} = 1000 Oe) were also carried out on a 53.5 mM frozen toluene solution of **1**, selected of the two compounds because of its high solubility, and the resulting data revealed analogous behavior to that of the polycrystalline sample (Figures S43, S44, and S47). The temperature dependent relaxation times for **1** and **5**, as well as the frozen solution sample of **1**, were best fit assuming a Raman-only relaxation process using the formula $\tau^{-1} = CT^n$ (see Table 3 for fit parameters). Kramers ions typically show a T^9 power dependence for Raman relaxation,[112] but other exponents have been found in practice,[26−29,113−115] due in part to the inadequacy of the Debye model in accurately modeling the phonon density distributions in molecular solids. Interestingly, the Raman fitting parameters differ for the polycrystalline and solution samples of **1**, which could reflect a change in the surrounding phonon (lattice vibration) environment in solution and removal of intermolecular interactions;

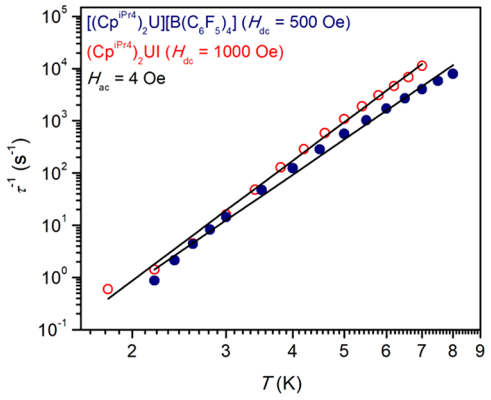

Figure 6. Plot of the relaxation rate (τ^{-1}) versus temperature (T) (log−log scale) for polycrystalline samples of $(Cp^{iPr4})_2UI$ (**1**) and $[(Cp^{iPr4})_2U][B(C_6F_5)_4]$ (**5**). Relaxation times for **1** were extracted from ac susceptibility measurements between 1.8 and 7.0 K, while those for **5** were extracted from measurements between 2.2 and 8.0 K. The red and blue circles represent the measured relaxation rates for **1** and **5**, respectively, while the black solid lines correspond to the best fit of the relaxation times according to the equation $\tau^{-1} = CT^n$.

Table 3. Parameters Used To Fit Temperature-Dependent Relaxation Times Extracted from Ac Magnetic Susceptibility Measurements on Polycrystalline 1, a 53.5 mM Frozen Toluene Solution of 1, and Polycrystalline 5[a]

parameter	polycrystalline **1**	frozen solution **1**	polycrystalline **5**
C ($K^{-n}\cdot s^{-1}$)	0.0044	0.0130	0.0058
n	7.63	6.53	6.98

[a]Data for **1** and **5** were collected under dc fields of 1000 and 500 Oe, respectively.

DOI: 10.1021/acs.inorgchem.9b02719
Inorg. Chem. 2019, 58, 16629−16641

however, the overall similarity in relaxation times and temperature dependence for both samples of **1** suggest that the origin of magnetic relaxation in **1** and, by extension, **5**, is molecular, arising principally through molecular-based vibrations constrained by the cyclopentadienyl ligands.

For the series $[(Cp^{iPr4X})_2Dy][B(C_6F_5)_4]$ (X = H, Me, Et, and ^{i}Pr), it was recently shown that slower relaxation dynamics and larger barriers to magnetic relaxation result with increasing Cp(cent)−Dy−Cp(cent) angle and strength of the Dy−Cp(cent) interaction.[28] In an interesting contrast, compound **5** exhibits a much smaller Cp(cent)−U−Cp(cent) angle than the recently reported single-molecule magnet $[(Cp^{iPr5})_2U][B(C_6F_5)_4]$[30] (142.5(2)° versus 167.82(8)°, respectively), although the applied-field relaxation times of **5** are an order of magnitude longer than those observed in the penta(isopropyl) analog. Computational studies suggest that the strong ligand field splitting in $[(Cp^{iPr5})_2U][B(C_6F_5)_4]$ results in significant quenching of the orbital angular momentum, which can facilitate efficient through-barrier relaxation.[105] Thus, the improved magnetic performance of **5** may arise from the more flexible coordination environment provided by Cp^{iPr4}, which results in a weaker ligand field splitting for the uranium center and hence a smaller quenching of the orbital angular momentum, as illustrated by the larger saturation magnetization of **5** relative to $[(Cp^{iPr5})_2U][B(C_6F_5)_4]$ (Figures S49−S51).

Despite the hypothetical potential for larger barriers to magnetic relaxation compared to those found in lanthanide complexes, the magnetization dynamics of **1** and **5** are dominated by through-barrier relaxation processes, as is typical of actinide systems. In contrast, the dysprosium analog of **5**, $[(Cp^{iPr4})_2Dy][B(C_6F_5)_4]$, was found to exhibit very slow magnetic relaxation, with a blocking temperature (corresponding to a 100-s relaxation time) of 17 K and an Orbach barrier of U_{eff} = 1285 cm^{-1}.[28] *Ab initio* spin dynamics calculations performed on $[Cp^{ttt}_2Dy][B(C_6F_5)_4]$ suggested that magnetic relaxation in this class of lanthanide compounds is predominately moderated by local molecular vibrations—specifically, bending modes within the Cp ligands.[27] The phonons arising from these vibrations provide the energy necessary for magnetic relaxation via a spin−phonon interaction, which is, in turn, facilitated by strong spin−orbit coupling.[116,117] In this context, the stronger spin−orbit coupling and metal−ligand interactions present in uranium species may make them more susceptible to strong spin−phonon interactions, and hence faster magnetic relaxation. This is further exacerbated by the low magnetic moment of uranium(III) relative to dysprosium(III), allowing for more intense mixing of excited magnetic states into the ground magnetic state, even in relatively high symmetries.[111]

CONCLUSIONS

Using the bulky tetra(isopropyl)cyclopentadienyl ligand, Cp^{iPr4}, we have synthesized the neutral uranium(III) compound $(Cp^{iPr4})_2UI$ (**1**), which serves as a reactant in synthesizing mononuclear uranium(IV) metallocene dihalides (**2-X**) and anionic uranium(III) metallocene dihalides (**3-X**) (for X^- = F^-, Cl^-, Br^-, and I^-). The dynamic behavior of the latter two series in solution was characterized using variable-temperature ^{1}H NMR spectroscopy, demonstrating that the size of the halide greatly affects the temperature at which the effective solution symmetry switches from C_{2v} to C_2. Cyclic voltammetric studies revealed that changing the halide ligands from chloride to fluoride shifts the uranium(III/IV) redox couple negatively by over half a volt, while only 130−160 mV shifts occur between the other neighboring sets of halide ligands. Similarly, a significantly greater change in the energy of the LMCT band in the uranium(IV) dihalides was observed between the chloride and the fluoride complexes. These results highlight the unique nature of the interactions between uranium and fluoride relative to the other halides.

Interestingly, it was also possible to synthesize the coordination solids **4-Cl** and **4-CN** from the reaction of **1** with CsCl and NaCN, respectively, in ethereal solvents. Finally, iodide abstraction from **1** yielded the "base-free" uranium(III) metallocenium cation salt (**5**) and its more stable DME adduct (**5-DME**). Complexes **1** and **5** exhibit similar magnetic relaxation behavior only under applied fields; however, this relaxation is slower than that of other reported mononuclear actinide single-molecule magnets, including the recently reported $[(Cp^{iPr5})_2U]^+$ cation. This slower relaxation can likely be ascribed to the generally more constrained ligand environment offered by the cyclopentadienyl coordination, while in the particular case of uranium, the greater flexibility of the Cp^{iPr4} ligand may serve to reduce anisotropy-quenching ligand field interactions. Even still, as these results demonstrate, the pervasiveness of through-barrier relaxation mechanisms continues to dramatically limit the performance of uranium single-molecule magnets compared to their lanthanide analogs.

Single-crystal X-ray diffraction characterization of all complexes in this work provided a unique opportunity to compare the effects of varying or abstracting halides and changing oxidation states on the solid-state structures of bent uranium metallocenes. In particular, this work provides experimental evidence for the prevalence of shallow potential energy wells in the Cp(cent)−U−Cp(cent) angle of these compounds. Efforts to isolate new reactive structures using the bulky but robust $(Cp^{iPr4})_2U$ fragment are ongoing.

ASSOCIATED CONTENT

Supporting Information

The Supporting Information is available free of charge at https://pubs.acs.org/doi/10.1021/acs.inorgchem.9b02719.

Experimental procedures, UV−vis data, NMR data, crystallographic data, electrochemical data, and magnetic data (PDF)

Accession Codes

CCDC 1942750−1942763 contain the supplementary crystallographic data for this paper. These data can be obtained free of charge via www.ccdc.cam.ac.uk/data_request/cif, or by emailing data_request@ccdc.cam.ac.uk, or by contacting The Cambridge Crystallographic Data Centre, 12 Union Road, Cambridge CB2 1EZ, UK; fax: +44 1223 336033.

AUTHOR INFORMATION

Corresponding Authors

*(J.A.) E-mail: arnold@berkeley.edu.
*(S.H.) E-mail: stephan.hohloch@upb.de.
*(J.R.L.) E-mail: jrlong@berkeley.edu.

ORCID

Michael A. Boreen: 0000-0001-7325-2717
Daniel J. Lussier: 0000-0002-6715-6443
Brighton A. Skeel: 0000-0001-8458-088X

DOI: 10.1021/acs.inorgchem.9b02719
Inorg. Chem. 2019, 58, 16629−16641

Trevor D. Lohrey: 0000-0003-3568-7861
David K. Shuh: 0000-0002-3104-3260
Jeffrey R. Long: 0000-0002-5324-1321
Stephan Hohloch: 0000-0002-5353-0801
John Arnold: 0000-0001-9671-227X

Notes

The authors declare no competing financial interest.

■ ACKNOWLEDGMENTS

This work was supported by the Director, Office of Science, Office of Basic Energy Sciences, Division of Chemical Sciences, Geosciences, and Biosciences Heavy Element Chemistry Program of the U.S. Department of Energy (DOE) at LBNL under Contract DE-AC02-05CH11231. Collection and interpretation of the magnetic data were supported by the National Science Foundation under NSF Grant CHE-1800252 to J.R.L. M.A.B. acknowledges support from the National Science Foundation Graduate Research Fellowship Program under Grant No. DGE 1106400. T.D.L. thanks the U.S. DOE Integrated University Program for a graduate research fellowship. S.H. thanks the Daimler and Benz Foundation (Grant No.: 32-06/17), the Fonds der chemischen Industrie (VCI), and Paderborn University for financial support of this work. We thank the College of Chemistry's NMR facility for resources provided and the staff for their assistance. Instruments in CoC-NMR are supported in part by NIH S10OD024998. The Advanced Light Source (ALS) is supported by the Director, Office of Science, Office of Basic Energy Sciences, of the U.S. DOE under Contract No. DE-AC02-05CH11231. Dr. Simon J. Teat is thanked for training and guidance throughout our crystallography work at the ALS. The authors thank Dr. Katie R. Meihaus for editorial assistance; Colin A. Gould, Dr. Philip C. Bunting, Dr. Wayne W. Lukens, Jr., Dr. Stefan Minasian, and Jeffrey S. Derrick for helpful discussions and Boulder Scientific Company for the donation of chemicals.

■ REFERENCES

(1) Liddle, S. T. The Renaissance of Non-Aqueous Uranium Chemistry. *Angew. Chem., Int. Ed.* **2015**, *54*, 8604.
(2) Ephritikhine, M. Recent Advances in Organoactinide Chemistry As Exemplified by Cyclopentadienyl Compounds. *Organometallics* **2013**, *32*, 2464.
(3) Cotton, F. A.; Wilkinson, G.; Murillo, C. A.; Bochmann, M. *Advanced Inorganic Chemistry*, 6th ed.; John Wiley & Sons: New York, 1999.
(4) Sharma, M.; Eisen, M. S. Metallocene Organoactinide Complexes. *Struct. Bonding (Berlin, Ger.)* **2008**, *127*, 1.
(5) Ventelon, L.; Lescop, C.; Arliguie, T.; Leverd, P. C.; Lance, M.; Nierlich, M.; Ephritikhine, M. Synthesis and X-ray crystal structure of $[Na(18\text{-crown-}6)][U(Cp^*)_2(SBu^t)(S)]$, the first f-element compound containing a metal−sulfur double bond. *Chem. Commun.* **1999**, 659.
(6) Arney, D. S. J.; Burns, C. J.; Smith, D. C. Synthesis and structure of the first uranium(VI) organometallic complex. *J. Am. Chem. Soc.* **1992**, *114*, 10068.
(7) Tourneux, J.-C.; Berthet, J.-C.; Thuéry, P.; Mézailles, N.; Le Floch, P.; Ephritikhine, M. Easy access to uranium nucleophilic carbene complexes. *Dalton Trans.* **2010**, *39*, 2494.
(8) Zi, G.; Jia, L.; Werkema, E. L.; Walter, M. D.; Gottfriedsen, J. P.; Andersen, R. A. Preparation and Reactions of Base-Free Bis(1,2,4-tri-*tert*-butylcyclopentadienyl)uranium Oxide, Cp'_2UO. *Organometallics* **2005**, *24*, 4251.
(9) Arney, D. S. J.; Burns, C. J. Synthesis and structure of high-valent organouranium complexes containing terminal monooxo functional groups. *J. Am. Chem. Soc.* **1993**, *115*, 9840.
(10) Evans, W. J.; Kozimor, S. A.; Ziller, J. W. Molecular Octa-Uranium Rings with Alternating Nitride and Azide Bridges. *Science* **2005**, *309*, 1835.
(11) Arney, D. S. J.; Burns, C. J. Synthesis and Properties of High-Valent Organouranium Complexes Containing Terminal Organoimido and Oxo Functional Groups. A New Class of Organo-f-Element Complexes. *J. Am. Chem. Soc.* **1995**, *117*, 9448.
(12) Altman, A. B.; Brown, A. C.; Rao, G.; Lohrey, T. D.; Britt, R. D.; Maron, L.; Minasian, S. G.; Shuh, D. K.; Arnold, J. Chemical structure and bonding in a thorium(III)−aluminum heterobimetallic complex. *Chem. Sci.* **2018**, *9*, 4317.
(13) Graves, C. R.; Kiplinger, J. L. Pentavalent uranium chemistry—synthetic pursuit of a rare oxidation state. *Chem. Commun.* **2009**, 3831.
(14) Graves, C. R.; Scott, B. L.; Morris, D. E.; Kiplinger, J. L. Facile Access to Pentavalent Uranium Organometallics: One-Electron Oxidation of Uranium(IV) Imido Complexes with Copper(I) Salts. *J. Am. Chem. Soc.* **2007**, *129*, 11914.
(15) Maynadié, J.; Barros, N.; Berthet, J.-C.; Thuéry, P.; Maron, L.; Ephritikhine, M. The Crucial Role of the f Electrons in the Bent or Linear Configuration of Uranium Cyanido Metallocenes. *Angew. Chem., Int. Ed.* **2007**, *46*, 2010.
(16) Graves, C. R.; Yang, P.; Kozimor, S. A.; Vaughn, A. E.; Clark, D. L.; Conradson, S. D.; Schelter, E. J.; Scott, B. L.; Thompson, J. D.; Hay, P. J.; Morris, D. E.; Kiplinger, J. L. Organometallic Uranium(V)−Imido Halide Complexes: From Synthesis to Electronic Structure and Bonding. *J. Am. Chem. Soc.* **2008**, *130*, 5272.
(17) Boisson, C.; Berthet, J.-C.; Lance, M.; Nierlich, M.; Vigner, J.; Ephritikhine, M. Synthesis of organouranium(V) compounds by oxidation of neutral tetravalent precursors. Crystal structures of $[U(\eta\text{-}C_5Me_5)(NMe_2)_3(OC_4H_8)][BPh_4]$ and $[U(\eta\text{-}C_5Me_5)_2(NEt_2)_2][BPh_4]$, the first cationic uranium(V) complexes. *J. Chem. Soc., Chem. Commun.* **1995**, 543.
(18) Murillo, J.; Fortier, S. Actinides: Pentavalent Organometallics. *Encyclopedia of Inorganic and Bioinorganic Chemistry* **2018**, 1.
(19) Boisson, C.; Berthet, J. C.; Ephritikhine, M.; Lance, M.; Nierlich, M. Synthesis and crystal structure of $[U(\eta\text{-}C_5Me_5)_2(OC_4H_8)_2][BPh_4]$, the first cationic cyclopentadienyl compound of uranium(III). *J. Organomet. Chem.* **1997**, *533*, 7.
(20) Evans, W. J.; Nyce, G. W.; Forrestal, K. J.; Ziller, J. W. Multiple Syntheses of $(C_5Me_5)_3U$. *Organometallics* **2002**, *21*, 1050.
(21) Duttera, M. R.; Fagan, P. J.; Marks, T. J.; Day, V. W. Synthesis, properties, and molecular structure of a trivalent organouranium diphosphine hydride. *J. Am. Chem. Soc.* **1982**, *104*, 865.
(22) Braunschweig, H.; Gackstatter, A.; Kupfer, T.; Radacki, K.; Franke, S.; Meyer, K.; Fucke, K.; Lemée-Cailleau, M.-H. Uranium Hydridoborates: Synthesis, Magnetism, and X-ray/Neutron Diffraction Structures. *Inorg. Chem.* **2015**, *54*, 8022.
(23) Evans, W. J.; Miller, K. A.; Kozimor, S. A.; Ziller, J. W.; DiPasquale, A. G.; Rheingold, A. L. Actinide Hydride Complexes as Multielectron Reductants: Analogous Reduction Chemistry from $[(C_5Me_5)_2UH]_2$, $[(C_5Me_5)_2UH_2]_2$, and $[(C_5Me_5)_2ThH_2]_2$. *Organometallics* **2007**, *26*, 3568.
(24) Evans, W. J.; Miller, K. A.; DiPasquale, A. G.; Rheingold, A. L.; Stewart, T. J.; Bau, R. A Crystallizable f-Element Tuck-In Complex: The Tuck-in Tuck-over Uranium Metallocene $[(C_5Me_5)U\{\mu\text{-}\eta^5\text{:}\eta^1\text{:}\eta^1\text{-}C_5Me_3(CH_2)_2\}(\mu\text{-}H)_2U(C_5Me_5)_2]$. *Angew. Chem., Int. Ed.* **2008**, *47*, 5075.
(25) Fagan, P. J.; Manriquez, J. M.; Maatta, E. A.; Seyam, A. M.; Marks, T. J. Synthesis and properties of bis(pentamethylcyclopentadienyl) actinide hydrocarbyls and hydrides. A new class of highly reactive f-element organometallic compounds. *J. Am. Chem. Soc.* **1981**, *103*, 6650.
(26) Guo, F.-S.; Day, B. M.; Chen, Y.-C.; Tong, M.-L.; Mansikkamäki, A.; Layfield, R. A. A Dysprosium Metallocene

DOI: 10.1021/acs.inorgchem.9b02719
Inorg. Chem. 2019, 58, 16629−16641

Single-Molecule Magnet Functioning at the Axial Limit. *Angew. Chem., Int. Ed.* **2017**, *56*, 11445.
(27) Goodwin, C. A. P.; Ortu, F.; Reta, D.; Chilton, N. F.; Mills, D. P. Molecular magnetic hysteresis at 60 K in dysprosocenium. *Nature* **2017**, *548*, 439.
(28) McClain, K. R.; Gould, C. A.; Chakarawet, K.; Teat, S. J.; Groshens, T. J.; Long, J. R.; Harvey, B. G. High-temperature magnetic blocking and magneto-structural correlations in a series of dysprosium(III) metallocenium single-molecule magnets. *Chem. Sci.* **2018**, *9*, 8492.
(29) Guo, F.-S.; Day, B. M.; Chen, Y.-C.; Tong, M.-L.; Mansikkamäki, A.; Layfield, R. A. Magnetic hysteresis up to 80 kelvin in a dysprosium metallocene single-molecule magnet. *Science* **2018**, *362*, 1400.
(30) Guo, F.-S.; Chen, Y.-C.; Tong, M.-L.; Mansikkamäki, A.; Layfield, R. Uranocenium: Synthesis, Structure, and Chemical Bonding. *Angew. Chem., Int. Ed.* **2019**, *58*, 10163.
(31) Sitzmann, H. Synthese von isopropylsubstituierten cyclopentadienylliganden. *J. Organomet. Chem.* **1988**, *354*, 203.
(32) Sitzmann, H.; Zhou, P.; Wolmershäuser, G. Titan-, Zirconium- und Hafniumkomplexe mit 1,2,4-Tri-*tert*-butylcyclopentadienyl-Liganden. *Chem. Ber.* **1994**, *127*, 3.
(33) Burkey, D. J.; Hays, M. L.; Duderstadt, R. E.; Hanusa, T. P. Synthesis, Structures, and Properties of "Encapsulated" Iron and Cobalt Metallocenes with Highly Isopropylated Cyclopentadienyl Rings. *Organometallics* **1997**, *16*, 1465.
(34) Quindt, V.; Saurenz, D.; Schmitt, O.; Schär, M.; Dezember, T.; Wolmershäuser, G.; Sitzmann, H. Bulky peralkylated cyclopentadienes by extension of Jutzi's pentamethylcyclopentadiene procedure. *J. Organomet. Chem.* **1999**, *579*, 376.
(35) Hays, M. L.; Burkey, D. J.; Overby, J. S.; Hanusa, T. P.; Sellers, S. P.; Yee, G. T.; Young, V. G. Steric Influence on the Structure, Magnetic Properties, and Reactivity of Hexa- and Octaisopropylmanganocene. *Organometallics* **1998**, *17*, 5521.
(36) Yao, S. A.; Martin-Diaconescu, V.; Infante, I.; Lancaster, K. M.; Götz, A. W.; DeBeer, S.; Berry, J. F. Electronic Structure of Ni_2E_2 Complexes (E = S, Se, Te) and a Global Analysis of M_2E_2 Compounds: A Case for Quantized E_2^{n-} Oxidation Levels with n = 2, 3, or 4. *J. Am. Chem. Soc.* **2015**, *137*, 4993.
(37) Bauer, H.; Weismann, J.; Saurenz, D.; Färber, C.; Schär, M.; Gidt, W.; Schädlich, I.; Wolmershäuser, G.; Sun, Y.; Harder, S.; Sitzmann, H. Chromocene, ferrocene, cobaltocene, and nickelocene derivatives with isopropyl and methyl or trimethylsilyl substituents. *J. Organomet. Chem.* **2016**, *809*, 63.
(38) Williams, R. A.; Tesh, K. F.; Hanusa, T. P. Encapsulated Alkaline-Earth Metallocenes. Synthesis, Solution Behavior, and Solid-State Structures of Bis(tetraisopropylcyclopentadienyl)calcium and -barium, $[(C_3H_7)_4C_5H]_2Ca$ and $[(C_3H_7)_4C_5H]_2Ba$. *J. Am. Chem. Soc.* **1991**, *113*, 4843.
(39) Burkey, D. J.; Hanusa, T. P. Synthesis and Characterization of the Encapsulated Stannocenes $[(C_3H_7)_3C_5H_2]_2Sn$ and $[(C_3H_7)_4C_5H]_2Sn$. *Organometallics* **1995**, *14*, 11.
(40) Sitzmann, H.; Weber, F.; Walter, M. D.; Wolmershäuser, G. Mono(alkylcyclopentadienyl) Complexes of Barium and Strontium. *Organometallics* **2003**, *22*, 1931.
(41) Sitzmann, H.; Dezember, T.; Schmitt, O.; Weber, F.; Wolmershäuser, G.; Ruck, M. Metallocenes of Samarium, Europium, and Ytterbium with the Especially Bulky Cyclopentadienyl Ligands $C_5H(CHMe_2)_4$, $C_5H_2(CMe_3)_3$, and $C_5(CHMe_2)_5$. *Z. Anorg. Allg. Chem.* **2000**, *626*, 2241.
(42) Visseaux, M.; Barbier-Baudry, D.; Blacque, O.; Hafid, A.; Richard, P.; Weber, F. New base-free metallocenes of samarium and neodymium, an approach to stereoelectronic control in organolanthanide chemistry. *New J. Chem.* **2000**, *24*, 939.
(43) Schmitt, O.; Wolmershäuser, G.; Sitzmann, H. The Substitution Reaction of (Chloro)bis(tetraisopropylcyclopentadienyl) Complexes of La, Pr, or Nd with Silylamides. *Eur. J. Inorg. Chem.* **2003**, *2003*, 3105.
(44) Sitzmann, H.; Schmitt, O.; Weber, F.; Wolmershäuser, G. Tetraisopropylcyclopentadienyl Chlorides of Lanthanum, Neodymium, and Ytterbium. *Z. Anorg. Allg. Chem.* **2001**, *627*, 12.
(45) Walter, M. D.; Bentz, D.; Weber, F.; Schmitt, O.; Wolmershäuser, G.; Sitzmann, H. Cation size dependent reactivity of lanthanide trihalides with bulky alkylcyclopentadienyl anions. *New J. Chem.* **2007**, *31*, 305.
(46) Barbier-Baudry, D.; Blacque, O.; Hafid, A.; Nyassi, A.; Sitzmann, H.; Visseaux, M. Synthesis and X-ray Crystal Structures of $(C_5HiPr_4)Ln(BH_4)_2(THF)$(Ln = Nd and Sm), Versatile Precursors for Polymerization Catalysts. *Eur. J. Inorg. Chem.* **2000**, *2000*, 2333.
(47) Cotton, S. *Lanthanide and Actinide Chemistry*; John Wiley & Sons: Chichester, U.K., 2006.
(48) Halter, D. P.; La Pierre, H. S.; Heinemann, F. W.; Meyer, K. Uranium(IV) Halide (F^-, Cl^-, Br^-, and I^-) Monoarene Complexes. *Inorg. Chem.* **2014**, *53*, 8418.
(49) Thomson, R. K.; Scott, B. L.; Morris, D. E.; Kiplinger, J. L. Synthesis, structure, spectroscopy and redox energetics of a series of uranium(IV) mixed-ligand metallocene complexes. *C. R. Chim.* **2010**, *13*, 790.
(50) Groom, C. R.; Bruno, I. J.; Lightfoot, M. P.; Ward, S. C. The Cambridge Structural Database. *Acta Crystallogr., Sect. B: Struct. Sci., Cryst. Eng. Mater.* **2016**, *B72*, 171.
(51) Clark, C. L.; Lockhart, J. J.; Fanwick, P. E.; Bart, S. C. Synthesis of low-valent uranium fluorides by C−F bond activation. *Chem. Commun.* **2015**, *51*, 14084.
(52) Garner, M. E.; Hohloch, S.; Maron, L.; Arnold, J. Carbon−Nitrogen Bond Cleavage by a Thorium-NHC-bpy Complex. *Angew. Chem., Int. Ed.* **2016**, *55*, 13789.
(53) Berthet, J.-C.; Thuéry, P.; Ephritikhine, M. Advances in f-element cyanide chemistry. *Dalton Trans.* **2015**, *44*, 7727.
(54) Chen, X.; Li, Q.; Gong, Y.; Andrews, L.; Liebov, B. K.; Fang, Z.; Dixon, D. A. Formation and Characterization of Homoleptic Thorium Isocyanide Complexes. *Inorg. Chem.* **2017**, *56*, 5060.
(55) Evans, W. J.; Mueller, T. J.; Ziller, J. W. Lanthanide versus Actinide Reactivity in the Formation of Sterically Crowded $[(C_5Me_5)_3ML_n]$ Nitrile and Isocyanide Complexes. *Chem. - Eur. J.* **2010**, *16*, 964.
(56) Maynadié, J.; Berthet, J.-C.; Thuéry, P.; Ephritikhine, M. Cyanide Metallocenes of Trivalent f-Elements. *Organometallics* **2007**, *26*, 2623.
(57) For comparison, the C−N stretch of NaCN was measured at 2080 cm^{-1}: Zhan, S.; Chen, X.; Vij, A.; Guo, D.; Meng, Q. Synthesis, studies and molecular structure of trinuclear cyanide-bridged copper−iron complexes. *Inorg. Chim. Acta* **1999**, *292*, 157.
(58) Connelly, S. J.; Kaminsky, W.; Heinekey, D. M. Structure and Solution Reactivity of (Triethylsilylium)triethylsilane Cations. *Organometallics* **2013**, *32*, 7478.
(59) See ref 45 for a discussion of the conformations of the Cp^{iPr4} ligand.
(60) Lichtscheidl, A. G.; Pagano, J. K.; Scott, B. L.; Nelson, A. T.; Kiplinger, J. L. Expanding the Chemistry of Actinide Metallocene Bromides. Synthesis, Properties and Molecular Structures of the Tetravalent and Trivalent Uranium Bromide Complexes: $(C_5Me_4R)_2UBr_2$, $(C_5Me_4R)_2U$(O-2,6-^{i}Pr$_2$C$_6$H$_3$)(Br), and $[K(THF)][(C_5Me_4R)_2UBr_2]$ (R = Me, Et). *Inorganics* **2016**, *4*, 1.
(61) Maynadié, J.; Berthet, J.-C.; Thuéry, P.; Ephritikhine, M. Bent and Linear Uranium(IV) Metallocenes with Terminal and Bridging Cyanide Ligands. *Organometallics* **2007**, *26*, 4585.
(62) Liptrot, D. J.; Power, P. P. London dispersion forces in sterically crowded inorganic and organometallic molecules. *Nat. Rev. Chem.* **2017**, *1*, 1.
(63) Hays, M. L.; Hanusa, T. P. Substituent Effects as Probes of Structure and Bonding in Mononuclear Metallocenes. *Adv. Organomet. Chem.* **1996**, *40*, 117.
(64) Timofeeva, T. V.; Lii, J.-H.; Allinger, N. L. Molecular Mechanics Explanation of the Metallocene Bent Sandwich Structure. *J. Am. Chem. Soc.* **1995**, *117*, 7452.

DOI: 10.1021/acs.inorgchem.9b02719
Inorg. Chem. 2019, 58, 16629−16641

(65) Shannon, R. D. Revised Effective Ionic Radii and Systematic Studies of Interatomic Distances in Halides and Chalcogenides. *Acta Crystallogr., Sect. A: Cryst. Phys., Diffr., Theor. Gen. Crystallogr.* **1976**, *A32*, 751.
(66) Blake, P. C.; Lappert, M. F.; Atwood, J. L.; Zhang, H. A Series of Bis(η-cyclopentadienyl)uranium(III) Dichloro-bridged-alkali-metal and Dihalogenobis(η-cyclopentadienyl)uranate(III) Complexes: Single-crystal *X*-ray Structure Determination of $[UCp''_2(\mu\text{-}Cl)_2Li(pmdeta)]$ and $[PPh_4][UCp''_2Cl_2]$[Cp″=η-$C_5H_3(SiMe_3)_2$-1,3, pmdeta = $(Me_2NCH_2CH_2)_2NMe$]. *J. Chem. Soc., Chem. Commun.* **1988**, 1436.
(67) Mehdoui, T.; Berthet, J.-C.; Thuéry, P.; Salmon, L.; Rivière, E.; Ephritikhine, M. Lanthanide(III)/Actinide(III) Differentiation in the Cerium and Uranium Complexes $[M(C_5Me_5)_2(L)]^{0,+}$ (L = 2,2′-Bipyridine, 2,2′:6′,2″-Terpyridine): Structural, Magnetic, and Reactivity Studies. *Chem. - Eur. J.* **2005**, *11*, 6994.
(68) Webster, C. L.; Langeslay, R. R.; Ziller, J. W.; Evans, W. J. Synthetic Utility of Tetrabutylammonium Salts in Uranium Metallocene Chemistry. *Organometallics* **2016**, *35*, 520.
(69) Lukens, W. W., Jr.; Beshouri, S. M.; Blosch, L. L.; Stuart, A. L.; Andersen, R. A. Preparation, Solution Behavior, and Solid-State Structures of $(1,3\text{-}R_2C_5H_3)_2UX_2$, Where R Is CMe_3 or $SiMe_3$ and X Is a One-Electron Ligand. *Organometallics* **1999**, *18*, 1235.
(70) Graves, C. R.; Schelter, E. J.; Cantat, T.; Scott, B. L.; Kiplinger, J. L. A Mild Protocol To Generate Uranium(IV) Mixed-Ligand Metallocene Complexes using Copper(I) Iodide. *Organometallics* **2008**, *27*, 5371.
(71) Evans, W. J.; Kozimor, S. A.; Ziller, J. W.; Fagin, A. A.; Bochkarev, M. N. Facile Syntheses of Unsolvated UI_3 and Tetramethylcyclopentadienyl Uranium Halides. *Inorg. Chem.* **2005**, *44*, 3993.
(72) Bauer, H.; Glöckner, A.; Tagne Kuate, A. C.; Schäfer, S.; Sun, Y.; Freytag, M.; Tamm, M.; Walter, M. D.; Sitzmann, H. How big is a Cp? Novel cycloheptatrienyl zirconium complexes with tri-, tetra- and pentasubstituted cyclopentadienyl ligands. *Dalton Trans.* **2014**, *43*, 15818.
(73) An earlier study[45] of lanthanide metallocene complexes observed that Cp^{iPr4} ligands are more flexible and accordingly can achieve closer contacts in bent metallocenes relative to Cp^{ttt}, leading the authors to describe the Cp^{ttt} as having "hard bulk" while Cp^{iPr4} exhibits "soft bulk".
(74) Dietrich, H. M.; Ziller, J. W.; Anwander, R.; Evans, W. J. Reactivity of $(C_5Me_5)_2UMe_2$ and $(C_5Me_5)_2UMeCl$ toward Group 13 Alkyls. *Organometallics* **2009**, *28*, 1173.
(75) Lukens, W. W., Jr.; Beshouri, S. M.; Stuart, A. L.; Andersen, R. A. Solution Structure and Behavior of Dimeric Uranium(III) Metallocene Halides. *Organometallics* **1999**, *18*, 1247.
(76) Blake, P. C.; Lappert, M. F.; Taylor, R. G.; Atwood, J. L.; Hunter, W. E.; Zhang, H. Synthesis, Spectroscopic Properties and Crystal Structures of $[ML_2Cl_2]$[M = Th or U; L = η-$C_5H_3(SiMe_3)_2$-1,3] and $[UL_2X_2]$(X = Br, I or BH_4). *J. Chem. Soc., Dalton Trans.* **1995**, 3335.
(77) Brennan, J. G.; Andersen, R. A.; Zalkin, A. Chemistry of Trivalent Uranium Metallocenes: Electron-Transfer Reactions with Carbon Disulfide. Formation of $[(RC_5H_4)_3U]_2[\mu\text{-}\eta^1,\eta^2\text{-}CS_2]$. *Inorg. Chem.* **1986**, *25*, 1756.
(78) Similar rotational restriction is observed in the ^{1}H NMR spectrum of $(Cp^{iPr5})_2UI$ at − 50 °C in toluene-d_8 but not in the ^{1}H NMR spectrum of $[(Cp^{iPr5})_2U][B(C_6F_5)_4]$ in CD_2Cl_2 at 30 °C. See ref 30.
(79) Robbins, J. L.; Edelstein, N.; Spencer, B.; Smart, J. C. Syntheses and electronic structures of decamethylmetallocenes. *J. Am. Chem. Soc.* **1982**, *104*, 1882.
(80) Chalkley, M. J.; Del Castillo, T. J.; Matson, B. D.; Peters, J. C. Fe-Mediated Nitrogen Fixation with a Metallocene Mediator: Exploring pK_a Effects and Demonstrating Electrocatalysis. *J. Am. Chem. Soc.* **2018**, *140*, 6122.
(81) Li, S.; Wei, M.; Huang, X.; Yang, X.-J.; Wu, B. Ion-pair induced self-assembly of molecular barrels with encapsulated tetraalkylammonium cations based on a bis−trisurea stave. *Chem. Commun.* **2012**, *48*, 3097.
(82) Turovskij, N. A.; Berestneva, Y. V.; Raksha, E. V.; Zubritskij, M. Y.; Grebenyuk, S. A. NMR study of the complex formation between *tert*-butyl hydroperoxide and tetraalkylammonium bromides. *Monatsh. Chem.* **2014**, *145*, 1443.
(83) Teichmann, J.; Bursch, M.; Köstler, B.; Bolte, M.; Lerner, H.-W.; Grimme, S.; Wagner, M. Trapping Experiments on a Trichlorosilanide Anion: a Key Intermediate of Halogenosilane Chemistry. *Inorg. Chem.* **2017**, *56*, 8683.
(84) La Mar, G. N. Ion Pairing and Interionic Distances in Some Paramagnetic Complexes from Proton Magnetic Resonance Spectra. *J. Chem. Phys.* **1965**, *43*, 235.
(85) Larsen, D. W.; Wahl, A. C. Nuclear Magnetic Resonance Study of Ion Association between Quaternary Ammonium Ions and Hexacyanoferrate(III) Ion. *Inorg. Chem.* **1965**, *4*, 1281.
(86) Taylor, R. P.; Kuntz, I. D., Jr. Ionic Interactions in Solution. I. Nuclear Magnetic Resonance Studies. *J. Am. Chem. Soc.* **1970**, *92*, 4813.
(87) Morris, D. E.; Da Re, R. E.; Jantunen, K. C.; Castro-Rodriguez, I.; Kiplinger, J. L. Trends in Electronic Structure and Redox Energetics for Early-Actinide Pentamethylcyclopentadienyl Complexes. *Organometallics* **2004**, *23*, 5142.
(88) Williams, U. J.; Carroll, P. J.; Schelter, E. J. Synthesis and Analysis of a Family of Cerium(IV) Halide and Pseudohalide Compounds. *Inorg. Chem.* **2014**, *53*, 6338.
(89) Straka, M.; Patzschke, M.; Pyykkö, P. Why are hexavalent uranium cyanides rare while U−F and U−O bonds are common and short? *Theor. Chem. Acc.* **2003**, *109*, 332.
(90) Wang, C.-Y.; Cheng, C.; Su, J.; Huai, P. Bonding nature of the actinide tetrafluorides AnF_4 (An = Th−Cm). *Mol. Phys.* **2015**, *113*, 3450.
(91) Graves, C. R.; Vaughn, A. E.; Schelter, E. J.; Scott, B. L.; Thompson, J. D.; Morris, D. E.; Kiplinger, J. L. Probing the Chemistry, Electronic Structure and Redox Energetics in Organometallic Pentavalent Uranium Complexes. *Inorg. Chem.* **2008**, *47*, 11879.
(92) Gu, S.; Wang, J.; Kaspar, R. B.; Fang, Q.; Zhang, B.; Coughlin, E. B.; Yan, Y. Permethyl Cobaltocenium ($Cp^*_2Co^+$) as an Ultra-Stable Cation for Polymer Hydroxide-Exchange Membranes. *Sci. Rep.* **2015**, *5*, 11668.
(93) Goodwin, C. A. P.; Reta, D.; Ortu, F.; Chilton, N. F.; Mills, D. P. Synthesis and Electronic Structures of Heavy Lanthanide Metallocenium Cations. *J. Am. Chem. Soc.* **2017**, *139*, 18714.
(94) Liu, J.; Reta, D.; Cleghorn, J. A.; Yeoh, Y. X.; Ortu, F.; Goodwin, C. A. P.; Chilton, N. F.; Mills, D. P. Light Lanthanide Metallocenium Cations Exhibiting Weak Equatorial Anion Interactions. *Chem. - Eur. J.* **2019**, *25*, 7749.
(95) Evans, P.; Reta, D.; Whitehead, G. F. S.; Chilton, N. F.; Mills, D. P. A *Bis*-Monophospholyl Dysprosium Cation Showing Magnetic Hysteresis at 48 K. *ChemRxiv Preprint*, 2019; https://chemrxiv.org/articles/A_Bis-Monophospholyl_Dysprosium_Cation_Showing_Magnetic_Hysteresis_at_48_Kelvin/10050128/1.
(96) Meihaus, K. R.; Long, J. R. Actinide-based single-molecule magnets. *Dalton Trans.* **2015**, *44*, 2517.
(97) Liddle, S. T.; van Slageren, J. Improving f-element single molecule magnets. *Chem. Soc. Rev.* **2015**, *44*, 6655.
(98) Magnani, N.; Caciuffo, R. Future Directions for Transuranic Single Molecule Magnets. *Inorganics* **2018**, *6*, 26.
(99) Coutinho, J. T.; Perfetti, M.; Baldoví, J. J.; Antunes, M. A.; Hallmen, P. P.; Bamberger, H.; Crassee, I.; Orlita, M.; Almeida, M.; van Slageren, J.; Pereira, L. C. J. Spectroscopic Determination of the Electronic Structure of a Uranium Single-Ion Magnet. *Chem. - Eur. J.* **2019**, *25*, 1758.
(100) Rinehart, J. D.; Meihaus, K. R.; Long, J. R. Observation of a Secondary Slow Relaxation Process for the Field-Induced Single-Molecule Magnet $U(H_2BPz_2)_3$. *J. Am. Chem. Soc.* **2010**, *132*, 7572.
(101) Meihaus, K. R.; Minasian, S. G.; Lukens, W. W., Jr.; Kozimor, S. A.; Shuh, D. K.; Tyliszczak, T.; Long, J. R. Influence of Pyrazolate

DOI: 10.1021/acs.inorgchem.9b02719
Inorg. Chem. 2019, 58, 16629−16641

vs *N*-Heterocyclic Carbene Ligands on the Slow Magnetic Relaxation of Homoleptic Trischelate Lanthanide(III) and Uranium(III) Complexes. *J. Am. Chem. Soc.* **2014**, *136*, 6056.
(102) Dey, S.; Velmurugan, G.; Rajaraman, G. How important is the coordinating atom in controlling magnetic anisotropy in uranium(III) single-ion magnets? A theoretical perspective. *Dalton Trans.* **2019**, *48*, 8976.
(103) Rinehart, J. D.; Long, J. R. Slow Magnetic Relaxation in a Trigonal Prismatic Uranium(III) Complex. *J. Am. Chem. Soc.* **2009**, *131*, 12558.
(104) Escalera-Moreno, L.; Baldoví, J. J.; Coronadoa, E. An efficient general methodology to explore the high-temperature frontier in f-block molecular nanomagnets. *arXiv:1905.06989v1. arXiv.org e-Print archive*. 2019; https://arxiv.org/abs/1905.06989v1.
(105) Guo, F.-S.; Bar, A. K.; Layfield, R. A. Main Group Chemistry at the Interface with Molecular Magnetism. *Chem. Rev.* **2019**, *119*, 8479.
(106) Kindra, D. R.; Evans, W. J. Magnetic Susceptibility of Uranium Complexes. *Chem. Rev.* **2014**, *114*, 8865.
(107) Edelstein, N. M.; Lander, G. H. Magnetic Properties. *The Chemistry of Actinides and Transactinide Elements* **2010**, *1*−*6*, 2225.
(108) Gatteschi, D.; Sessoli, R.; Villain, J. *Molecular Nanomagnets*; Oxford University Press: Oxford, U.K., 2006.
(109) Werncke, C. G.; Bunting, P. C.; Duhayon, C.; Long, J. R.; Bontemps, S.; Sabo-Etienne, S. Two-Coordinate Iron(I) Complex $[Fe\{N(SiMe_3)_2\}_2]^-$: Synthesis, Properties, and Redox Activity. *Angew. Chem., Int. Ed.* **2015**, *54*, 245.
(110) Harriman, K. L. M.; Le Roy, J. J.; Ungur, L.; Holmberg, R. J.; Korobkov, I.; Murugesu, M. Cycloheptatrienyl trianion: an elusive bridge in the search of exchange coupled dinuclear organolanthanide single-molecule magnets. *Chem. Sci.* **2017**, *8*, 231.
(111) Escalera-Moreno, L.; Baldoví, J. J.; Gaita-Ariño, A.; Coronado, E. Exploring the High-Temperature Frontier in Molecular Nanomagnets: From Lanthanides to Actinides. *Inorg. Chem.* **2019**, *58*, 11883.
(112) Abragam, A.; Bleany, B. *Electron Paramagnetic Resonance of Transition Ions*; Dover Publications, Inc.: 1986.
(113) Rechkemmer, Y.; Breitgoff, F. D.; van der Meer, M.; Atanasov, M.; Hakl, M.; Orlita, M.; Neugebauer, P.; Neese, F.; Sarkar, B.; van Slageren, J. A four-coordinate cobalt(II) single-ion magnet with coercivity and a very high energy barrier. *Nat. Commun.* **2016**, *7*, 10467.
(114) Yao, X.-N.; Du, J.-Z.; Zhang, Y.-Q.; Leng, X.-B.; Yang, M.-W.; Jiang, S.-D.; Wang, Z.-X.; Ouyang, Z.-W.; Deng, L.; Wang, B.-W.; Gao, S. Two-Coordinate Co(II) Imido Complexes as Outstanding Single-Molecule Magnets. *J. Am. Chem. Soc.* **2017**, *139*, 373.
(115) Novikov, V. V.; Pavlov, A. A.; Nelyubina, Y. V.; Boulon, M.-E.; Varzatskii, O. A.; Voloshin, Y. Z.; Winpenny, R. E. P. A Trigonal Prismatic Mononuclear Cobalt(II) Complex Showing Single-Molecule Magnet Behavior. *J. Am. Chem. Soc.* **2015**, *137*, 9792.
(116) Lunghi, A.; Totti, F.; Sessoli, R.; Sanvito, S. The role of anharmonic phonons in under-barrier spin relaxation of single molecule magnets. *Nat. Commun.* **2017**, *8*, 14620.
(117) Lunghi, A.; Totti, F.; Sanvito, S.; Sessoli, R. Intra-molecular origin of the spin-phonon coupling in slow-relaxing molecular magnets. *Chem. Sci.* **2017**, *8*, 6051.

DOI: 10.1021/acs.inorgchem.9b02719
Inorg. Chem. 2019, 58, 16629−16641